

Growth Mechanism and Morphology of Hexagonal Boron Nitride

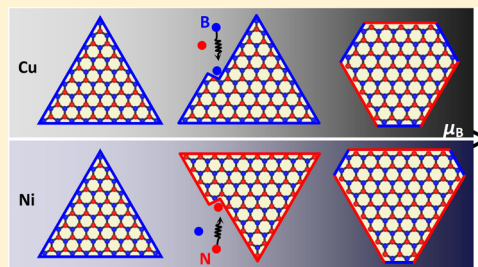
Zhuhua Zhang, Yuanyue Liu, Yang Yang, and Boris I. Yakobson*

Department of Materials Science and NanoEngineering and Department of Chemistry, Rice University, Houston, Texas 77005, United States

S Supporting Information

ABSTRACT: Hexagonal boron nitride (h-BN) sheet is a structural analogue of graphene, yet its growth mechanism has been rarely studied, as complicated by its binary composition. Here, we reveal an atomistic growth mechanism for the h-BN islands by combining crystal growth theory with comprehensive first-principles calculations. The island shapes preferred by edge equilibrium are found to be inconsistent with experimental facts, which is in contrast to previous common views. Then the growth kinetics is explored by analyzing the diffusion and docking of boron and nitrogen atoms at the edges in a step-by-step manner of the nanoreactor approach. The determined sequence of atom-by-atom accretion reveals a strong kinetic anisotropy of growth. Depending on the chemical potential of constituent elements, it yields the h-BN shapes as equilateral triangles or hexagons, explaining a number of experimental observations and opening a way for the synthesis of quality h-BN with controlled morphology. The richer growth kinetics of h-BN compared to graphene is further extendable to other binary two-dimensional materials, notably metal dichalcogenides.

KEYWORDS: Hexagonal boron nitride, Wulff construction, morphology, crystal growth, kinetics, density functional theory calculations



Two-dimensional (2D) hexagonal boron nitride (h-BN) has attracted interest due to a number of exceptional properties^{1–4} and applications as, for example, dielectric material for flexible nanoelectronics,^{5,6} oxidation-resistant coating,^{7–9} and ultraviolet optics material.^{1,10,11} The technological potential of h-BN, however, is severely limited by the lack of scalable growth of large-area, high-quality sheets. Progress has been achieved mainly through chemical vapor deposition (CVD) on various substrates, including the mostly used Cu^{3,12–19} and Ni^{20–24} as well as noble Ru,^{25,26} Pt,^{27–29} and other substrates.^{30–32} Fundamental to better CVD growth of 2D h-BN is the understanding of its mechanism. A common feature for the CVD growth of 2D materials is that the feeding units produced by decomposed precursor first bind to substrate-catalyst and then migrate to the edge of material lattice. The detailed atom-by-atom sequence of accretion to the growing lattice is crucial to the quality and morphology of the product. Previous theory has demonstrated that such non-equilibrium kinetics near the frontier of growing graphene is definitive to the growth anisotropy, the island morphology, and the suppressed formation of defects,^{33,34} well explaining a number of experimental phenomena. However, the situation is quite different for the h-BN due to its (i) lower lattice symmetry and (ii) binary composition. First, the lack of inversion symmetry in h-BN not only leads to a richer variety of its edges but also complicates the very definition of edge energy.^{35,36} Second, an extra degree of freedom in the Gibbs phase rule unties the chemical potential balance between B and N, adding variability to h-BN growth. Third, the atom-by-atom sequence of atom accretion to the h-BN lattice is inherently more complicated because having two chemical constituents

largely broadens the possibilities for accretion sequences. Furthermore, the h-BN island shapes have been observed to vary from regular triangles^{12–24} to truncated triangles²³ and even to hexagons.¹⁹ These issues and evident features call for the development of growth theory views “beyond (mono-elemental) graphene”.

Here, we report the atomistic growth mechanism for the h-BN based on crystal growth theory augmented with detailed first-principles calculations, as in our nanoreactor approach.³³ First, we establish the edge structures and calculate the energies for all edge directions to determine the equilibrium shape of h-BN islands, which varies depending on chemical potential of B (μ_B) and mostly differs from the triangles^{12–24} or hexagons^{19,23} seen in experiments. This contrasts with earlier common views,^{14–21,37,38} that the h-BN island shapes are established thermodynamically. We thus turn to growth kinetics at h-BN edges. The calculated nucleation barriers of atomic rows allow us to evaluate the growth rates for different edge directions, which reveal strong kinetic anisotropy of growth, shaping the BN islands into N-terminated triangles that have been identified in several experiments.^{21,39} With increasing μ_B , the islands evolve into truncated triangles or hexagons, reproducing the shapes in other experiments.^{19,40} Of more interest is the formation of B-terminated triangles on Ni at high chemical potential of feeding units, which calls for experimental verification. On the basis of the prototypic nature of considered systems, our analyses should be transferable to other binary 2D

Received: November 30, 2015

Revised: January 23, 2016

Published: January 26, 2016

materials, while also guiding the synthesis of quality h-BN sheets with controlled morphology.

The model systems consist of h-BN nanostructures placed on metal substrate of three atomic layers. Here we considered two metal surfaces, Cu(111) and Ni(111), both common for CVD synthesis of h-BN. Nanoribbons on metal are used to calculate the energy of armchair edges as well as the energy of atom accretion to different edges, whereas triangular clusters, also on metal, are needed to calculate the energies of zigzag edges. The h-BN sheet is stretched by 1.6% on Cu and compressed by 0.9% on Ni to make them commensurate. All the first-principles calculations are performed with the Vienna ab initio Simulation Package (VASP) code^{41,42} with the projector-augmented wave method for the potential at the core region and spin-polarized density functional theory (DFT) based on the generalized gradient approximation of Perdew–Burke–Ernzerhof (PBE) functional.⁴³ A kinetic energy cutoff of 400 eV is chosen for the plane-wave expansion. In all structures, the vacuum region between two adjacent periodic images is fixed to 10 Å to eliminate spurious interaction. The Brillouin-zone integration is sampled at the Γ point only. The positions of metal atoms of the top two layers plus the entire BN structures are relaxed using the conjugate-gradient method until the force on each atom is less than 0.01 eV/Å.

We start our analysis from h-BN edges on metals, the prerequisite for obtaining the equilibrium island shapes. Like graphene, the h-BN sheet has two principal edges, the armchair (A) and zigzag (Z). The lack of inversion symmetry splits the Z edge into two types, terminated by B (Z_B) and N (Z_N), Figure 1a. We measure the edge direction angle χ from the A edge, so

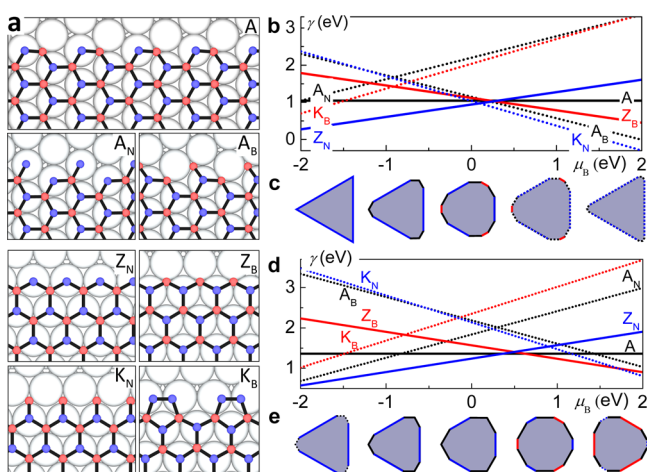


Figure 1. Edges and equilibrium shapes of h-BN on metal. (a) Edges of h-BN sheet on Ni, including standard armchair (A), B- and N-terminated zigzag (Z_B and Z_N) edges as well as their reconstructed versions. (b,d) Edge energy of h-BN on Ni (b) and on Cu (d) versus chemical potential of boron, μ_B . (c,e) Equilibrium shapes of h-BN on Ni (c) and on Cu (e) at $\mu_B = -1.0, -0.5, 0, 0.5,$ and 1.0 eV (from left to right). The perimeter lines in black, red, and blue solid and blue and black dotted stand for the A, Z_B , Z_N , K_N and A_B (A_N on Cu) edges, respectively.

that for Z_N edge $\chi = -30^\circ$ and for Z_B edge $\chi = 30^\circ$. The edge energy γ for an arbitrary direction χ can be approximately obtained from those of basic directions^{36,44}

$$\gamma(\chi) = |\gamma| \cos(\chi + C) \quad (1)$$

where $|\gamma| = 2(\gamma_A^2 + \gamma_{Zx}^2 - \sqrt{3}\gamma_A\gamma_{Zx})^{1/2}$ and $C = \text{sgn}(\chi) \cdot \arctan(\sqrt{3-2\gamma_{Zx}/\gamma_A})$ with the subscript x being N for $-30^\circ < \chi < 0$ and B for $0 < \chi < 30^\circ$. γ_{Zx} and γ_A are the energies of Z_x and A edges on metals that can be calculated by

$$\gamma = \gamma_f - E_b \quad (2)$$

where γ_f is the edge energy of freestanding h-BN sheet, and E_b is the binding energy between the BN edge and metal. γ_f has been determined in our previous work³⁶ and can be directly adopted here. E_b for the A edge can be calculated as $E_b = (E_{\text{sys}} - E_{\text{ribbon}} - E_{\text{substrate}})/2L$, where E_{sys} is the energy of the whole system of an armchair ribbon bound to metal, E_{ribbon} and $E_{\text{substrate}}$ are the energies of two constituents, separately, and L is the edge length, expressed always in units of h-BN lattice constant (2.50 Å). E_b for the A edge is 0.86 eV on Ni and 0.54 eV on Cu, per lattice constant of h-BN. However, the same method applied to the Z edge yields only the average E_b of the opposite Z_B and Z_N edges. To determine E_b for each Z edge separately, we use a series of triangular BN islands with only Z_B or Z_N edges, stacked on metals in the same registry. The total binding energy of the island has three contributions: the edges, corners, and the interior lattice.^{35,36} With increasing island size, the edge part increases linearly, while the corner part is a constant and the interior part is negligible due to weak interaction between the h-BN and metals. Fitting the total binding energy of a series of islands into a linear function of island size results in E_b for the Z_B and Z_N edges, which are 1.5 and 1.7 eV on Cu and 2.0 and 1.9 eV on Ni, respectively (see details in Figure S1). The average E_b of Z_B and Z_N edges agrees with that (e.g., 1.97 eV on Ni) obtained using the ribbon model, validating our method based on BN triangles.

The substrate may change the ground-state structures of the edges, as exemplified by graphene on metals.^{33,45} Accordingly, we explore edge-reconstructions for h-BN, as illustrated in Figure 1a. Following the graphene edge reconstruction, we modify the A edge by attaching extra B (N) atoms to it, denoted as A_B (A_N); we also attach extra N (B) atoms to the Z_B (Z_N) edges, to design the Klein forms,⁴⁶ denoted here as K_B (K_N). Energies of these edges on metal substrates, γ' , can be calculated by

$$\gamma' = \gamma + (E_{\text{sys}}' - E_{\text{sys}} - x\mu_B - y\mu_N) / L \quad (3)$$

where E_{sys}' is the total energy of the whole system of a BN ribbon with one reconstructed edge bound to metal, E_{sys} is the energy of the same system but with standard ribbon edges (i.e., A edge or Z_B and Z_N edges), x and y are the numbers of extra B and N atoms at the reconstructed edge with respect to the standard edge, and μ_B and μ_N are the elemental chemical potentials.

For the h-BN, unlike graphene, edge energies do not have specific values but depend on the chemical potential offset between B and N, especially for the Z and Klein edges, which are always compositionally unbalanced. The chemical potentials of B and N satisfy $\mu_B + \mu_N = \mu_{\text{BN}}^0 + \Delta\mu_{\text{BN}}$, where μ_{BN}^0 is the energy of a BN pair in a h-BN sheet on metal, and $\Delta\mu_{\text{BN}}$ represents the degree of nonequilibrium. We first consider the near thermodynamic equilibrium case and set $\Delta\mu_{\text{BN}} = 0.01$ eV. Still, individual μ_B and μ_N remain uncertain. To choose a specific condition, one can assume that the B and N species arrive to the substrate in equal quantity/concentration, having thus similar entropy, yet they bind with different strengths E_B and E_N , which mainly determine the difference in their chemical potentials

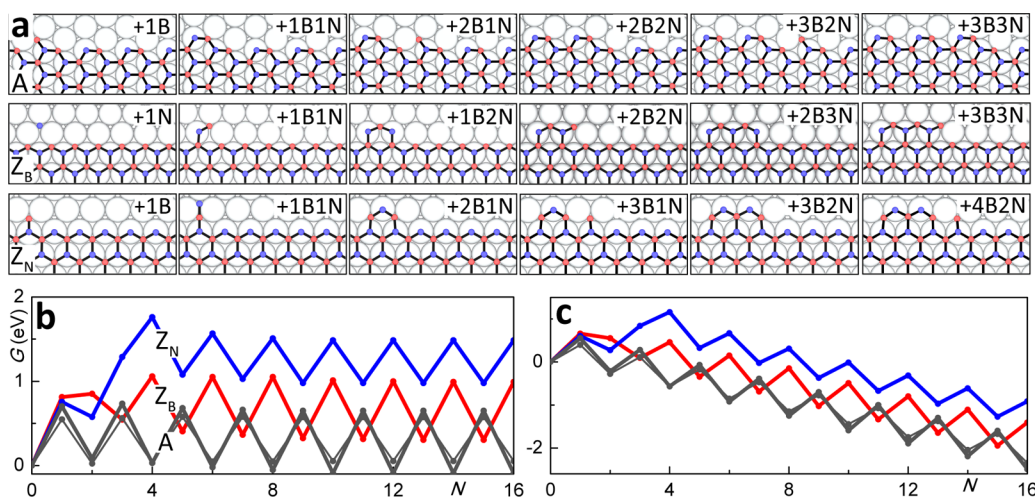


Figure 2. Kinetic models of h-BN growth on Ni. (a) Optimal atomic configurations during the docking of B and N monomers to the A (top), Z_B (middle), and Z_N (bottom) edges at $\mu_B = -0.5$ eV. (b,c) Corresponding free energy evolution at $\Delta\mu_{BN} = 0.01$ (b) and 0.3 eV (c). Gray thin line represents the kink-flow growth along a skewed (6,1) near- Z_B edge.

$$\mu_B - \mu_N = -E_B + E_N \quad (4)$$

We use these μ_B and μ_N values as reference and discuss how the h-BN growth can be controlled by varying the chemical potential.

With these provisions, we calculate the energies of standard and reconstructed edges on Ni and Cu, as shown in Figure 1b,d, respectively. The energies of all edges other than the A exhibit linear slope with μ_B , proportional to the excess of B atoms at the edge. Among the standard edges, the Z_N is energetically favored at N-rich condition, whereas the Z_B is preferred at B-rich. However, at very low μ_B (i.e., high μ_N) extra N atoms can be attached to reconstruct the Z_B edge into more stable K_B edge. Alike, B attachment at high μ_B favorably alters the Z_N edge into K_N edge and the A edge into A_B edge. On Ni, the N atoms at the K_B edge dimerize to form pentagons while the B atoms at the K_N edge remain disconnected with each other. This is attributed to a distinctly stable stacking registry of h-BN on Ni(111) in which the N atoms are located directly above the surface Ni atoms while the B atoms are strongly bound on face-centered cubic (fcc) surface sites (see Figure 1a). Thus, the N atoms of the K_B edge are weakly bound to Ni, allowing them to dimerize. In contrast, no dimerization is found at the Klein edges on Cu as all the edge atoms are strongly bound on the fcc sites on Cu (Figure S2).

Having determined the edge energies, we can obtain the thermodynamic Wulff construction,⁴⁷ as shown in Figures 1c (in Ni) and 1e (in Cu). The equilibrium shape of h-BN strongly depends on μ_B . On Ni, at N-rich condition the BN shape is a triangle solely with Z_N edges. At greater μ_B , the shape first evolves into a nonagon with dominant Z_N edges and a small portion of A, and then into a dodecagon with added Z_B . Further increase of μ_B holds the dodecagon shape, yet with the Z_N and A edges replaced by K_N and A_B edges, respectively. At very high μ_B , the shape restores to a nonagon enclosed by the K_N and A_B edges. The BN shape on Cu exhibits similar evolution, from nonagon at B-rich condition to dodecagon at N-rich condition. These equilibrium shapes, either on Ni or Cu, mostly differ from the observed triangular^{12–24} and hexagonal^{19,23} h-BN islands in experiments, which motivates us to explore the growth kinetics.

The kinetic shape is built based on the growth velocities $\nu(\gamma)$ in each direction, determined by the process of atomic accretion to the corresponding edges. According to the ideas of step-flow growth of crystals,⁴⁸ each edge moves forward by incorporating atoms arriving to its active sites. It is important to know the preferred states of arriving atoms and their dynamics on metals before they dock to the edge. We consider three species, B and N monomers and BN dimer. On Ni, the most stable adsorption site for the B monomer is the subsurface octahedral site, whereas the preferred site for the N monomer is the fcc surface site. The barriers for the B and N diffusion on Ni are 0.12 and 0.29 eV, respectively, indicating their high mobility at practical growth temperatures ($T \sim 1000$ – 1400 K, or $k_B T \sim 0.09$ – 0.12 eV). The BN dimer is 0.03 eV lower in energy than a pair of isolated B and N, but it has much higher diffusion barrier of 0.98 eV. Plus, under growth condition the increased entropy should further favor the monomers with respect to dimers. Therefore, the monomers should be the dominant species for h-BN growth on Ni. The situation is different on Cu, where a dimer is more stable than the isolated monomers by 1.59 eV. Yet, the diffusion barrier on Cu is as low as 0.09 eV for the B monomer and 0.14 eV for the N monomer, compared to that of 0.80 eV for the BN dimer. We thus speculate that the monomers and dimers both contribute to the h-BN growth on Cu.

On the basis of the above, we first assume B and N monomers as feeding units in considering the growth kinetics on Ni and will extend the results to BN dimers later. We start with $\mu_B = -0.5$ eV at which the A, Z_B , and Z_N edges are most stable for their respective directions. B and N atoms are sequentially added to these edges. Unlike graphene, h-BN allows two options, B or N, for each step of attachment. Multiple configurations are considered for each step to ensure the whole structure always has the lowest free energy at chosen chemical condition. The formation of B–B or N–N bonds at the edges proves to be unfavorable as it raises the energy of system. Also, the states containing topological defects, such as pentagon or 5/7, are all suppressed because these defects not only contain unavoidable homoelemental bonds but also cause additional strain (see Figure S3). Protrusions at the edges are higher in energy as well, and therefore any branching into dendrites is unfavorable, unless the chemical potential μ_{BN} is

sufficiently high to allow their formation. This possibility may explain the h-BN triangles with sawtooth edges,³⁰ grown by exposing the Si-doped iron surface to undiluted borazine (this gives high μ_{BN}).

Figure 2a presents the evolution of lowest-energy atomic configurations during the docking of atoms to the A, Z_B, and Z_N edges on Ni (the results on Cu are provided in Figure S4), all free of defects, homoelemental bonds, and protrusions. At the A edge, B atom is preferred to be the first for nucleating a new atomic row, and then N and B atoms are docked alternatively to advance the row. Similar sequence occurs to the Z_B edge. The nucleation is different at the Z_N edge, where a group of 3 B and 1 N forms initially and then is followed by alternating attachment of N and B atoms. Figure 2b presents the free energy evolution during the growth of A, Z_B, and Z_N edges at $\mu_{\text{B}} = 0$ eV. The growth kinetics of h-BN exhibits strong anisotropy. The free energy barrier is $E_{\text{N}}^* = 1.76$ eV high for nucleating an atomic row at the Z_N edge, lowers to $E_{\text{B}}^* = 1.06$ eV at the Z_B edge, and is merely $E_{\text{A}}^* = 0.73$ eV at the A edge. After a few steps of atom addition, the energy profiles evolve into a periodic up–down alternating level sequences with the amplitudes being close to that of kink-flow growth (Figure 2b, dashed line). The stages of growth at BN edges comprises two steps: the nucleation of a new atomic row and then the sequential addition of atoms to the kink sites, similar to graphene growth.³³ However, for h-BN the kinetics exhibits several important features, as shown in Figure 3 (also in Figure

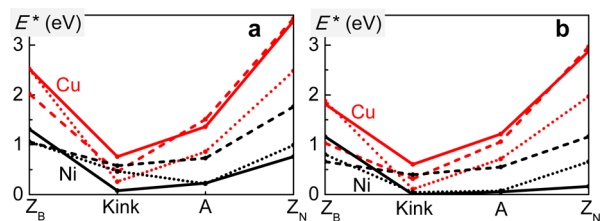


Figure 3. Free energy barriers for nucleating atomic rows at principal h-BN edges. (a) Kinetic barrier of growth at $\mu_{\text{B}} = -0.5$ eV (dashed lines), 0 eV (solid lines), and 0.5 eV (dotted lines) on Cu (red lines) and Ni (black lines) at $\Delta\mu_{\text{BN}} = 0.01$ eV. (b) The same as (a) but at $\Delta\mu_{\text{BN}} = 0.3$ eV.

S5 for different μ_{B}) summarizing the row nucleation barriers at the principal BN edges. First, the Z_B and Z_N edges show apparently different barriers, and their difference, $E_{\text{N}}^* - E_{\text{B}}^*$, changes broadly with μ_{B} , from 0.7 eV at $\mu_{\text{B}} = -0.5$ eV to -0.55 eV at $\mu_{\text{B}} = 0$ eV and to -0.07 eV at $\mu_{\text{B}} = 0.5$ eV on Ni. On Cu, $E_{\text{N}}^* - E_{\text{B}}^*$ monotonically decreases from 1.51 eV at $\mu_{\text{B}} = -0.5$ eV to -0.4 eV at $\mu_{\text{B}} = 0.5$ eV. These results suggest tunable growth anisotropy by controlling the chemical states of the feedstock. Second, all the row nucleation barriers generally decrease with increasing μ_{B} , indicative of faster growth of h-BN sheet under B-richer condition even though μ_{BN} is fixed to almost equilibrium value. Third, varying μ_{B} changes not only the row nucleation barrier but also the sequences of atom accretion at the edges (Figure S6), leading to nonlinear dependence of $E_{\text{N}}^* - E_{\text{B}}^*$ on μ_{B} . At last, the row nucleation barriers at all the edges depend on metal, with the values on Ni being nearly half of those on Cu, which is in contrast to graphene growth in which only the barrier at the Z edge is sensitive to metal.³³

With the row-nucleation energy barriers determined, the direction-dependent h-BN growth velocity can be calculated by

$$\begin{aligned} v(\chi) \propto & 2s_{\text{A}}(\chi)\exp[(-E_{\text{A}}^* + \Delta\mu_{\text{BN}})/kT] \\ & + (s_{\text{Z}}(\chi) - [s_{\text{K}}(\chi) - s_{\text{K}}^0(\chi)])\exp[(-E_{\text{Z}}^* + \Delta\mu_{\text{BN}}) \\ & /kT] + 2s_{\text{K}}(\chi)\exp[(-E_{\text{K}}^* + \Delta\mu_{\text{BN}})/kT] \end{aligned} \quad (5)$$

where $s_{\text{A}}(\chi)$, $s_{\text{Z}}(\chi)$, and $s_{\text{K}}(\chi)$ are concentrations of active sites at A and Z edge-segments and kinks, and $s_{\text{K}}^0(\chi)$ is the concentration of intrinsic kinks on the edges. The detailed expression for these quantities can be found in our earlier work.³³ Here, the lack of inversion symmetry of h-BN sheet can be accounted by setting E_{Z}^* to E_{N}^* at $-30^\circ < \chi < 0^\circ$ and to E_{B}^* at $0^\circ < \chi < 30^\circ$. Then, the kinetic Wulff construction can be obtained based on growth velocity as a function of χ and is shown in Figures 4 and S7. At the kinetic control, the effect of

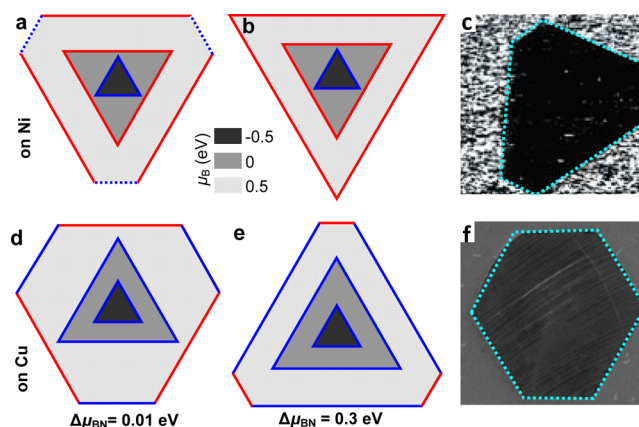


Figure 4. Shapes determined by kinetic Wulff construction for h-BN on Ni (a,b) and on Cu (d,e) at selected μ_{B} , and $k_{\text{B}}T = 0.1$ eV. The results at $\Delta\mu_{\text{BN}} = 0.01$ eV are shown in (a,d), and the results at $\Delta\mu_{\text{BN}} = 0.3$ eV are in (b,e). The red, blue, and black lines represent the standard Z_B, Z_N, and A edges (dashed blue is the K_N edge). Polar plots of growth velocity $\nu(\chi)$ are shown in Figure S9. Experimental images are shown for comparison, a truncated h-BN triangle on Ni (c) (Reprinted with permission from ref 21, copyright 2003 Elsevier) and a h-BN hexagon on Cu (f) (Reprinted with permission from ref 19, copyright 2014 American Chemical Society).

asymmetry on the growth is amplified^{33,34} because $\nu(\chi)$ depends on energy barriers exponentially, which is in contrast to the equilibrium shapes that depend on the edge energy linearly. Thus, the “rounded” polygons (e.g. nonagon and dodecagon) derived from equilibrium become unlikely if the regime is kinetic. On Ni, at $\mu_{\text{B}} = -0.5$ eV, the A, Z_B, and all skewed edges grow much faster than Z_N, resulting in a triangular h-BN island enclosed by Z_N edges (Figure 4a, inmost), consistent with the shapes often observed in experiments. At $\mu_{\text{B}} = 0$ eV, the shape is still triangular but is inverted, enclosed by B-terminated edges. This counters the often assumed N-termination for the BN triangles^{37,38} and calls for clarification on the edge orientation of h-BN domains on Ni. Further higher $\mu_{\text{B}} = 0.5$ eV leads the B-terminated triangle to be truncated by new K_N edges, as illustrated in Figure 4a outmost shape. Notably, the truncated BN triangle has also been observed experimentally (Figure 4c).²³ On Cu, the N-terminated h-BN triangle prevails in the region of low and moderate μ_{B} , but it evolves into a hexagon with alternating Z_B and Z_N edges at high μ_{B} (Figure 4d). This provides an insight for understanding the h-BN hexagons synthesized on electroplished Cu (Figure 4f) by Tay et al.¹⁹ According to the XPS

analyses,¹⁹ the polished Cu surface has been considerably oxidized, which weakens the binding of supported atoms and may correspond to a case of high μ_B . In actual growth, different substrates may also affect the BN shapes, as exemplified by the growth on Ru(0001), which interacts stronger with the N edges than with the B edges and results in almost exclusively N-terminated BN triangles.³⁹ Moreover, hydrogen also plays an important yet poorly understood role in the h-BN growth; it may deplete active sites at the edges, thus increasing the atom diffusion along the edge, adjusting the grow rate.⁴⁹ Fully understanding these factors requires further study.

Upon raising $\Delta\mu_{\text{BN}}$ to a moderate value of 0.3 eV, the free energy of the edge growth displays an overall decrease with sequential atom attachment (Figure 2c). Yet, the row nucleation barriers remain, and the kinetic anisotropy of growth appears to be more pronounced. At B-rich condition, E_B^* is distinctly higher than E_N^* for the growth on Ni, compared to the $\Delta\mu_{\text{BN}} = 0.01$ eV case, while the opposite holds on Cu (Figure 3b). As a result, the BN triangles with B-terminated edges can grow in a wider range of μ_B on Ni while the BN shapes on Cu are enclosed more dominantly by N-terminated edges (Figure 4b,e).

If the feeding units were provided as a mixture of monomers and dimers, the results would be essentially the same (see Figure S7). In that case, attaching dimers may skip the heights in the free energy profiles and therefore reduce the row nucleation barriers for all the edges, but the kinetic anisotropy of growth is unaffected. If the feeding units were provided exclusively in the form of BN dimers, the standard A, Z_B , and Z_N edges would be energetically preferred over the reconstructed edges, and their growth kinetics would be independent of μ_B ; the significantly higher barrier at the Z_N edge than those at the other edges results solely in the N-terminated triangles on both metals, as illustrated by kinetic Wulff construction in Figure S8.

In summary, combining crystal growth theory with detailed atomistic calculations, we have determined the atomistic growth mechanism for 2D h-BN sheets. We show that the equilibrium shape of BN islands strongly depends on the chemical state of the feedstock but mostly differs from experimental triangle or hexagon shapes, which is in contrast to previous views that the commonly produced BN triangles are thermodynamically defined. This led us to explore the nonequilibrium kinetics at the edges. The determined sequence of atomic row assembly at the edges with suppressed defect formation shows strong kinetic anisotropy of growth. An advantage of h-BN growth is that its kinetics can be controlled by adjusting the chemical balance between B and N. At N-rich condition, the growth at the zigzag N-edge needs to overcome a substantial nucleation barrier and becomes the slowest among all edge directions, thereby shaping the h-BN islands into N-terminated triangles. Under B-rich condition, the BN shapes on Cu can evolve into truncated triangles or hexagons with additional B-terminated edges, resembling those obtained in several experiments, whereas the h-BN islands on Ni can be B-terminated triangles, which calls for clarification of the edge orientation for synthesized h-BN triangles. Our results provide the first atomistic picture for the growth of 2D binary materials and will serve as a useful guidance for controlled synthesis of quality layers or even desirable shapes of hybrids h-BN/C.⁵⁰ The analysis should be transferable to the growth of other binaries, notably of metal dichalcogenides.

■ ASSOCIATED CONTENT

Supporting Information

The Supporting Information is available free of charge on the ACS Publications website at DOI: 10.1021/acs.nanolett.5b04874.

Binding energy of h-BN triangles on metals, optimized edge structures of h-BN on Cu, free energy for the defect formation during growth, kinetic models of h-BN growth on Cu, effect of μ_B on free energy evolution during the atom docking, optimal atomic configurations during the atom docking to BN edges on Cu, kinetic growth of h-BN based on mixed feeding units of monomers and dimers, and kinetic Wulff construction for h-BN on metals at different μ_B are collected. (PDF)

■ AUTHOR INFORMATION

Corresponding Author

*E-mail: biy@rice.edu.

Notes

The authors declare no competing financial interest.

■ ACKNOWLEDGMENTS

The authors thank Vasilii I. Artyukhov and Qinghong Yuan for helpful discussions. This work was supported by the Department of Energy, BES Grant DE-SC0001479 and (case of Cu substrate only) the research fund of the SKL-MCMS in NUAU, Grant MCMS-0415K01. Computer resources were provided by XSEDE under allocation TG-DMR100029 and TG-DMR150091 and the DAVinCI cluster.

■ REFERENCES

- (1) Watanabe, K.; Taniguchi, T.; Kanda, H. *Nat. Mater.* **2004**, *3*, 404–409.
- (2) Zeng, H.; Zhi, C.; Zhang, Z.; Wei, X.; Wang, X.; Guo, W.; Bando, Y.; Golberg, D. *Nano Lett.* **2010**, *10*, 5049–5055.
- (3) Song, L.; Ci, L.; Lu, H.; Sorokin, P. B.; Jin, C.; Ni, J.; Kvashnin, A. G.; Kvashnin, D. G.; Lou, J.; Yakobson, B. I.; Ajayan, P. M. *Nano Lett.* **2010**, *10*, 3209–3215.
- (4) Zhang, Z.; Guo, W. *Phys. Rev. B: Condens. Matter Mater. Phys.* **2008**, *77*, 075403.
- (5) Salvatore, G. A.; Münzenrieder, N.; Barraud, C.; Petti, L.; Zysset, C.; Büthe, L.; Ensslin, K.; Tröster, G. *ACS Nano* **2013**, *7*, 8809–8815.
- (6) Dean, C.; Young, A.; Meric, I.; Lee, C.; Wang, L.; Sorgenfrei, S.; Watanabe, K.; Taniguchi, T.; Kim, P.; Shepard, K. *Nat. Nanotechnol.* **2010**, *5*, 722–726.
- (7) Husain, E.; Narayanan, T. N.; Taha-Tijerina, J. J.; Vinod, S.; Vajtai, R.; Ajayan, P. M. *ACS Appl. Mater. Interfaces* **2013**, *5*, 4129–4135.
- (8) Liu, Z.; Gong, Y.; Zhou, W.; Ma, L.; Yu, J.; Idrobo, J. C.; Jung, J.; MacDonald, A. H.; Vajtai, R.; Lou, J. *Nat. Commun.* **2013**, *4*, 2541.
- (9) Li, X.; Yin, J.; Zhou, J.; Guo, W. *Nanotechnology* **2014**, *25*, 105701.
- (10) Watanabe, K.; Taniguchi, T.; Niyama, T.; Miya, K.; Taniguchi, M. *Nat. Photonics* **2009**, *3*, 591–594.
- (11) Kubota, Y.; Watanabe, K.; Tsuda, O.; Taniguchi, T. *Science* **2007**, *317*, 932–934.
- (12) Kim, K. K.; Hsu, A.; Jia, X.; Kim, S. M.; Shi, Y.; Hofmann, M.; Nezich, D.; Rodriguez-Nieva, J. F.; Dresselhaus, M.; Palacios, T. *Nano Lett.* **2012**, *12*, 161–166.
- (13) Yin, J.; Yu, J.; Li, X.; Li, J.; Zhou, J.; Zhang, Z.; Guo, W. *Small* **2015**, *11*, 4497–4502.
- (14) Lu, G.; Wu, T.; Yuan, Q.; Wang, H.; Wang, H.; Ding, F.; Xie, X.; Jiang, M. *Nat. Commun.* **2015**, *6*, 6160.
- (15) Lee, K. H.; Shin, H.-J.; Lee, J.; Lee, I.-y.; Kim, G.-H.; Choi, J.-Y.; Kim, S.-W. *Nano Lett.* **2012**, *12*, 714–718.

- (16) Wang, L.; Wu, B.; Chen, J.; Liu, H.; Hu, P.; Liu, Y. *Adv. Mater.* **2014**, *26*, 1559–1564.
- (17) Khan, M. H.; Huang, Z.; Xiao, F.; Casillas, G.; Chen, Z.; Molino, P. J.; Liu, H. K. *Sci. Rep.* **2015**, *5*, 7743.
- (18) Čavar, E.; Westerström, R.; Mikkelsen, A.; Lundgren, E.; Vinogradov, A.; Ng, M. L.; Preobrajenski, A.; Zakharov, A.; Mårtensson, N. *Surf. Sci.* **2008**, *602*, 1722–1726.
- (19) Tay, R. Y.; Griep, M. H.; Mallick, G.; Tsang, S. H.; Singh, R. S.; Tumlin, T.; Teo, E. H. T.; Karna, S. P. *Nano Lett.* **2014**, *14*, 839–846.
- (20) Auwärter, W.; Suter, H. U.; Sachdev, H.; Greber, T. *Chem. Mater.* **2004**, *16*, 343–345.
- (21) Auwärter, W.; Muntwiler, M.; Osterwalder, J.; Greber, T. *Surf. Sci.* **2003**, *545*, L735–L740.
- (22) Shi, Y.; Hamsen, C.; Jia, X.; Kim, K. K.; Reina, A.; Hofmann, M.; Hsu, A. L.; Zhang, K.; Li, H.; Juang, Z.-Y. *Nano Lett.* **2010**, *10*, 4134–4139.
- (23) Chatterjee, S.; Luo, Z.; Acerce, M.; Yates, D. M.; Johnson, A. C.; Sneddon, L. G. *Chem. Mater.* **2011**, *23*, 4414–4416.
- (24) Gibb, A. L.; Alem, N.; Chen, J.-H.; Erickson, K. J.; Ciston, J.; Gautam, A.; Linck, M.; Zettl, A. *J. Am. Chem. Soc.* **2013**, *135*, 6758–6761.
- (25) Sutter, P.; Lahiri, J.; Zahl, P.; Wang, B.; Sutter, E. *Nano Lett.* **2013**, *13*, 276–281.
- (26) Sutter, P.; Lahiri, J.; Albrecht, P.; Sutter, E. *ACS Nano* **2011**, *5*, 7303–7309.
- (27) Kim, G.; Jang, A.-R.; Jeong, H. Y.; Lee, Z.; Kang, D. J.; Shin, H. S. *Nano Lett.* **2013**, *13*, 1834–1839.
- (28) Müller, F.; Stöwe, K.; Sachdev, H. *Chem. Mater.* **2005**, *17*, 3464–3467.
- (29) Gao, Y.; Ren, W.; Ma, T.; Liu, Z.; Zhang, Y.; Liu, W.-B.; Ma, L.-P.; Ma, X.; Cheng, H.-M. *ACS Nano* **2013**, *7*, 5199–5206.
- (30) Caneva, S.; Weatherup, R. S.; Bayer, B. C.; Brennan, B.; Spencer, S. J.; Mingard, K.; Cabrero-Vilatela, A.; Baehtz, C.; Pollard, A. J.; Hofmann, S. *Nano Lett.* **2015**, *15*, 1867–1875.
- (31) Zhang, C.; Fu, L.; Zhao, S.; Zhou, Y.; Peng, H.; Liu, Z. *Adv. Mater.* **2014**, *26*, 1776–1781.
- (32) Yin, J.; Liu, X.; Lu, W.; Li, J.; Cao, Y.; Li, Y.; Xu, Y.; Li, X.; Zhou, J.; Jin, C. *Small* **2015**, *11*, 5375–5380.
- (33) Artyukhov, V. I.; Liu, Y.; Yakobson, B. I. *Proc. Natl. Acad. Sci. U. S. A.* **2012**, *109*, 15136–15140.
- (34) Artyukhov, V. I.; Hao, Y.; Ruoff, R. S.; Yakobson, B. I. *Phys. Rev. Lett.* **2015**, *114*, 115502.
- (35) Rapcewicz, K.; Chen, B.; Yakobson, B.; Bernholc, J. *Phys. Rev. B: Condens. Matter Mater. Phys.* **1998**, *57*, 7281–7291.
- (36) Liu, Y.; Bhowmick, S.; Yakobson, B. I. *Nano Lett.* **2011**, *11*, 3113–3116.
- (37) Ismach, A.; Chou, H.; Ferrer, D. A.; Wu, Y.; McDonnell, S.; Floresca, H. C.; Covacevich, A.; Pope, C.; Piner, R.; Kim, M. J. *ACS Nano* **2012**, *6*, 6378–6385.
- (38) Orofeo, C. M.; Suzuki, S.; Kageshima, H.; Hibino, H. *Nano Res.* **2013**, *6*, 335–347.
- (39) Lu, J.; Yeo, P. S. E.; Zheng, Y.; Xu, H.; Gan, C. K.; Sullivan, M. B.; Castro Neto, A. H.; Loh, K. P. *J. Am. Chem. Soc.* **2013**, *135*, 2368–2373.
- (40) Stehle, Y.; Meyer, H. M.; Unocic, R. R.; Kidder, M.; Polizos, G.; Datskos, P. G.; Jackson, R.; Smirnov, S. N.; Vlassioug, I. V. *Chem. Mater.* **2015**, *27*, 8041–8047.
- (41) Kresse, G.; Hafner, J. *Phys. Rev. B: Condens. Matter Mater. Phys.* **1994**, *49*, 14251–14269.
- (42) Kresse, G.; Furthmüller, J. *Phys. Rev. B: Condens. Matter Mater. Phys.* **1996**, *54*, 11169–11186.
- (43) Perdew, J. P.; Burke, K.; Ernzerhof, M. *Phys. Rev. Lett.* **1996**, *77*, 3865–3868.
- (44) Liu, Y.; Dobrinsky, A.; Yakobson, B. I. *Phys. Rev. Lett.* **2010**, *105*, 235502.
- (45) Gao, J.; Zhao, J.; Ding, F. *J. Am. Chem. Soc.* **2012**, *134*, 6204–6209.
- (46) Wagner, P.; Ivanovskaya, V. V.; Melle-Franco, M.; Humbert, B.; Adjizian, J.-J.; Briddon, P. R.; Ewels, C. P. *Phys. Rev. B: Condens. Matter Mater. Phys.* **2013**, *88*, 094106.
- (47) Herring, C. *Phys. Rev.* **1951**, *82*, 87–93.
- (48) Burton, W.-K.; Cabrera, N.; Frank, F. *Philos. Trans. R. Soc., A* **1951**, *243*, 299–358.
- (49) Vlassioug, I.; Regmi, M.; Fulvio, P.; Dai, S.; Datskos, P.; Eres, G.; Smirnov, S. *ACS Nano* **2011**, *5*, 6069–6076.
- (50) Bhowmick, S.; Singh, A. K.; Yakobson, B. I. *J. Phys. Chem. C* **2011**, *115*, 9889–9893.
- (51) Zhao, R.; Li, F.; Liu, Z.; Liu, Z.; Ding, F. *Phys. Chem. Chem. Phys.* **2015**, *17*, 29327–29334.
- (52) Drost, R.; Kezilebieke, S.; Ervasti, M. M.; Hamalainen, S. K.; Schulz, F.; Harju, A.; Liljeroth, P. *Sci. Rep.* **2015**, *5*, 16741.

NOTE ADDED IN PROOF

After the submission of our manuscript, we note a related work,⁵¹ focused on the equilibrium h-BN shapes. Another report⁵² brought to our attention shows triangular and hexagonal h-BN domains embedded in graphene.³⁶